

000 ROBUST BIDIRECTIONAL ASSOCIATIVE MEMORY 001 002 VIA REGULARIZATION INSPIRED BY 003 004 THE SUBSPACE ROTATION ALGORITHM 005

006 **Anonymous authors**

007 Paper under double-blind review

011 ABSTRACT

013 Bidirectional Associative Memory (BAM) trained by Bidirectional Backpropagation (B-BP) suffer from poor robustness and sensitivity to noise and adversarial
014 attacks. To address it, we propose a novel gradient-free training algorithm, the
015 Bidirectional Subspace Rotation Algorithm (B-SRA), designed to improve the
016 robustness and convergence behavior of BAM. Through comprehensive experi-
017 ments, two key principles, orthogonal weight matrices (OWM) and gradient-pattern
018 alignment (GPA), are identified as central to enhancing the robustness of BAM.
019 Motivated by these insights, new regularization strategies are introduced into
020 B-BP, yielding models with significantly improved resistance to corruption and
021 adversarial perturbations. We conduct an ablation study across different training
022 strategies to determine which approach achieves a more robust BAM. Additionally,
023 we evaluate the robustness of BAM under various attack scenarios and across
024 increasing memory capacities, including the association of 50, 100, and 200 pattern
025 pairs. Among all strategies, the SAME configuration—which combines OWM and
026 GPA—achieves the highest resilience. Our findings suggest that B-SRA and care-
027 fully designed regularization strategies lead to more reliable associative memories
028 and open new directions for building resilient neural architectures.

031 1 INTRODUCTION

033 Over the past decades, numerous researchers have sought to enhance the robustness, stability, and
034 retrieval fidelity of associative memory (AM). Early studies investigated noise-tolerant learning
035 rules and stability analyses (Feng & Plumondon, 2003; Leung et al., 1995; Hassoun & Watta, 2020),
036 while others explored improved bidirectional mapping mechanisms and energy-based formulations to
037 reduce retrieval errors (Giles & Maxwell, 1987; Acevedo-Mosqueda et al., 2013). More recent work
038 has examined AM under adversarial and uncertain environments, highlighting vulnerability to noise
039 and perturbations in both theoretical and practical settings (Karunaratne et al., 2021; Zhang & Zeng,
040 2023). Techniques for enhancing stability, such as regularization, pruning strategies, and biologically
041 inspired learning rules, have also been proposed to improve resilience under challenging conditions
042 (Strock et al., 2020).

043 Despite these efforts, BAM trained via gradient-based methods such as Bidirectional Backpropagation
044 (B-BP) (Adigun & Kosko, 2019; Kosko, 2021; Rosenblatt et al., 1962) still suffer from several major
045 limitations. These include slow convergence, high sensitivity to initialization and hyperparameters,
046 and vulnerability to noise and adversarial attacks. Such weaknesses hinder the deployment of
047 BAM in real-world applications, particularly those requiring robustness under uncertainty, such as
048 biometric authentication (Zhang & Yang, 2023), autonomous systems (Hsu et al., 2023), and secure
049 communications (Paraiso et al., 2021).

050 Recent advances in associative memory architectures, such as Dense Associative Memories (DAM)
051 (Krotov & Hopfield, 2016) and Modern Hopfield Networks (MHN) (Ramsauer et al., 2022), offer
052 increased capacity and stability. However, both DAM and MHN function more like feedforward
053 neural networks rather than true BAM when it comes to pattern retrieval. The challenge of achieving
robust associative retrieval, particularly under noisy or adversarial conditions, remains unresolved.

054 1.1 MOTIVATION AND CONTRIBUTION
055

056 Traditionally, B-BP is a popular algorithm for training BAM (Adigun & Kosko, 2019). Inspired by
057 recent advances in training associative memories through subspace rotation techniques (Lin et al.,
058 2024; 2023; 2025), we extend SRA from RHN to BAM. Specifically, we propose the Bidirectional
059 Subspace Rotation Algorithm (B-SRA), a novel, gradient-free training method that enhances the
060 robustness and convergence speed of BAM by directly optimizing their weight matrices through
061 subspace rotation, thus avoiding the limitations of gradient-based approaches like B-BP. Inspired by
062 BAM trained by B-SRA, we further proposed two regularization that could improve the robustness of
063 BAM significantly. The key contributions of this paper are summarized as follows:

- 064 • **Extension of SRA to BAM:** We have proposed the Bidirectional Subspace Rotation Algo-
065 rithm (B-SRA), a gradient-free training method for BAM, which accelerates convergence
066 and enhances robustness against adversarial attacks.
- 067 • **Introduction of Regularization to B-BP:** By analyzing the behavior of BAM trained with
068 B-SRA, we propose two regularizers—Orthogonal Weight Matrix (OWM) and Gradient-
069 Pattern Alignment (GPA)—and incorporate them into B-BP to improve the robustness of
070 BAM.
- 071 • **Evaluation of BAM Robustness Against Adversarial Attacks:** The performance of BAM
072 trained with B-SRA, B-BP, and B-BP regularized with OWM and GPA is evaluated under
073 several adversarial attacks, including the Fast Gradient Sign Method (FGSM) (Goodfellow
074 et al., 2014), Fast FGSM (FFGSM) (Wong et al., 2020), Basic Iterative Method (BIM) (Ku-
075 rakin et al., 2018), Projected Gradient Descent (PGD) (Madry et al., 2017), and Gaussian
076 Noise (GN).
- 077

078 1.2 ORGANIZATION
079

080 The rest of the paper is organized as follows: In Section 2, we introduce the definition of BAM and
081 describe its dynamical behavior in detail. In Section 3, we discuss the underlying mechanism of the
082 Subspace Rotation Algorithm (SRA) and propose B-SRA for training BAM. Section 4 presents a
083 comprehensive experimental evaluation of BAM trained using different strategies, including B-BP,
084 B-SRA, and B-BP with the proposed regularizers. We analyze robustness under various conditions,
085 such as corrupted inputs, GN, and adversarial attacks (FGSM, FFGSM, BIM, PGD). Finally, in
086 Section 5, we conclude that B-SRA outperforms B-BP in training a robust BAM. Inspired by B-SRA,
087 B-BP With the OWM and GPA regularizations can further enhance the resilience of BAM under
088 various adversarial attacks.

090 2 BIDIRECTIONAL ASSOCIATIVE MEMORY
091

092 Assuming we have a BAM with K layers, meaning we have K layers of weight matrix, which are
093 indexed as W_1, W_2, \dots, W_K . The paired patterns are called A and B. Without loss of generality, let
094 the input pattern A be considered as the first hidden layer 0 and the input pattern B as the last hidden
095 layer K , so the layers can be indexed as h_0, h_1, \dots, h_K .

096 In the path from pattern A to pattern B, the signal before activation is represented by U , indexed as
097 U_1, U_2, \dots, U_K , and the signal after activation is represented by H , indexed as H_0, H_1, \dots, H_K .
098 Note that H_0 is actually the input pattern A. In the path from pattern B back to pattern A, the
099 reconstructed signal before activation is represented by R , indexed as R_K, \dots, R_0 , corresponding to
100 U_1, U_2, \dots, U_K , and the signal after activation is represented by V , indexed as V_K, V_{K-1}, \dots, V_1 ,
101 corresponding to H_0, H_1, \dots, H_K .

102 The dynamical behavior of the BAM can then be described as follows:

103 **In the Path from A End to B End:**

$$104 \frac{dU_k(t)}{dt} = W_k H_{k-1}(t), \quad H_k(t) = g \odot (U_k(t)), \quad k = 1, 2, \dots, K. \quad (1)$$

108 where $U_k(t)$ is the pre-activation state of layer k , and $H_k(t)$ is the post-activation state computed
 109 using a non-linear activation function $g \odot (\cdot)$, which is an element-wise operation and is chosen as
 110 tanh in our study. W_k is the weight matrix at layer K . The state $U_k(t)$ evolves dynamically over time
 111 as the input $H_{k-1}(t)$ propagates through the network, producing the output $H_k(t)$ for each layer.
 112

113 **In the Path from B End to A End:**

114

$$115 \frac{dR_{k-1}(t)}{dt} = V_k(t)W_k^T, \quad V_{k-1}(t) = g \odot (R_{k-1}(t)), \quad k = K, \dots, 1. \quad (2)$$

116

117 where $R_k(t)$ is the pre-activation state of layer k , and $V_k(t)$ is the post-activation state computed
 118 using $g \odot (\cdot)$, which is also an element-wise operation and is chosen as tanh in our study. W_k^T is the
 119 transpose of the weight matrix for backward signals at layer k . In this context, it is necessary to keep
 120 it mind that V_K is equivalent to H_K , and R_0 is equivalent to H_0 .
 121

122 **2.1 STABILITY ANALYSIS**

123

124 To analyze the dynamical stability of the BAM, we define an energy function $E(t)$ that decreases
 125 monotonically over time during inference. The energy function encompasses contributions from both
 126 paths: the path from the A end to the B end and the path from the B end to the A end, representing
 127 the interaction of states, weights, biases, and their temporal dynamics, as shown in Equation 3.
 128

$$129 E(t) = -\frac{1}{2} \sum_{k=1}^K V_k(t)^T W_k H_{k-1}(t) \quad (3)$$

130

132 The time derivative of the energy function can be expressed in Equation 4.

133

$$134 \frac{dE(t)}{dt} = -\frac{1}{2} \sum_{k=1}^K \left[\left(\frac{dV_k(t)}{dt} \right)^T W_k H_{k-1}(t) + V_k(t)^T W_k \left(\frac{dH_{k-1}(t)}{dt} \right) \right] \quad (4)$$

135

138 Using the dynamics described by the path from the A end to the B end, as shown in Equation 1,
 139 and the backward path, as shown in Equation 2, the derivative can be further expanded as shown in
 140 Equation 5.

141

$$142 \frac{dE(t)}{dt} = -\frac{1}{2} \sum_{k=1}^K \left[\left(\frac{dV_k(t)}{dt} \right)^T \frac{dU_k(t)}{dt} + \left(\frac{dR_{k-1}(t)}{dt} \right)^T \frac{dH_{k-1}(t)}{dt} \right] \quad (5)$$

143

145 Then, furthermore, we could obtain the Equation 6.

146

$$147 \frac{dE(t)}{dt} = -\frac{1}{2} \sum_{k=1}^K \left[(g \odot (R_k(t))' \left(\frac{dR_k(t)}{dt} \right)^T \frac{dU_k(t)}{dt} + (g \odot (U_{k-1}(t))' \left(\frac{dR_{k-1}(t)}{dt} \right)^T \frac{dU_{k-1}(t)}{dt}) \right] \quad (6)$$

148

149 Since the activation function $g \odot (\cdot)$ is tanh, sigmoid, or ReLU, it satisfies $\frac{dg}{dt} \geq 0$. Meanwhile,
 150 R_k and U_k are at the same layer, and their rates of change have the same sign. Therefore, the inner
 151 product of their derivatives is greater than zero. As a result, we have $\frac{dE(t)}{dt} \leq 0$.
 152

153 This implies that the energy function $E(t)$ does not increase with time, ensuring the dynamical
 154 stability of the BAM during inference. The network evolves toward a stable equilibrium, minimizing
 155 the energy function during its operation.

156

157 **3 BIDIRECTIONAL SUBSPACE ROTATION ALGORITHM**

158

159 **3.1 MATHEMATICAL MECHANISM FOR BIDIRECTIONAL SUBSPACE ROTATION ALGORITHM**

160

161 In analyzing the mathematical mechanism of BAM, let us start with the most fundamental and original
 162 BAM, $Y = \text{sign}(WX)$, $X = \text{sign}(W^T Y)$.

162 For randomly initialized \hat{W} , the outputs are \hat{Y} and \hat{X} respectively. Now, the question becomes how
 163 can we rotate the \hat{W} to make the distance between Y and \hat{Y} and X and \hat{X} minimum. Then we need
 164 to optimize the Equation 7.
 165

$$\min_{Q^T Q = I_p} \|Y - \hat{Y}Q\|_F + \|X - \hat{X}Q^T\|_F \quad (7)$$

166
 167 Please refer to Appendix B for details on how this objective is achieved using subspace rotation
 168 algorithm.
 169

172 3.2 PSEUDO-CODE FOR B-SRA AND B-BP WITH TWO REGULARIZERS

174 In practice, BAM is normally a non-linear system, but the underlying mechanism is the same as
 175 described in the Section 3.1. However, we will find the optimization subspace for A and B end
 176 alternatively. Then finally, both ends will reach its minimum value. According to the mathematical
 177 mechanism mentioned in Section 3.1, we could deduce the B-SRA, as shown in the following pseudo-
 178 algorithm 1. While, the B-BP with OWM and GPA regularizers are shown in pseudo-algorithm
 179 2.
 180

181 **Algorithm 1** Bidirectional Subspace Rotation Algorithm

182 **Input:** Samples X, Y, N(Number of Layers) ,and the Epoch
 183 **Output:** weight matrix W_{ix} and W_{iy}
 184 **Initialization:** Initialize the orthogonal weight matrices W_{ix} and W_{iy} . For convenience, the two
 185 ends of the BAM are referred to as follows: the input end X is called A, and the input end Y is
 186 called B. The symbol \times indicates matrix multiplication in this algorithm; we write it explicitly to
 187 clearly show the process.
 188 **for** index $\leftarrow 1$ to Epoch **do**
 189 Train the BAM from the central weight matrix to the weight matrix at the end
 190 Alternatively, update the weight matrix at the A end and the weight matrix at the B end
 191 **for** Counter $\leftarrow 1$ to N/2 **do**
 192 Train the Weight Matrix Closed to A End Firstly
 193 $\hat{A}_{ix} = \text{A_FORWARD_B}(X, \text{layer}=ix)$
 194 $\hat{H}_{ix} = \text{B_FORWARD_A}(Y, \text{layer}=ix)$
 195 $U, \Sigma, V \leftarrow \text{SVD}(\hat{A}_{ix}^T \times \hat{H}_{ix})$
 196 $W_{ix} \leftarrow U \times V \times W_{ix}$
 197 Train the Weight Matrix Closed to B End Secondly
 198 $iy = N - ix$
 199 $\hat{B}_{iy} = \text{B_FORWARD_A}(Y, \text{layer}=iy)$
 200 $\hat{H}_{iy} = \text{A_FORWARD_B}(X, \text{layer}=iy)$
 201 $U, \Sigma, V \leftarrow \text{SVD}(\hat{B}_{iy}^T \times \hat{H}_{iy})$
 202 $W_{iy} \leftarrow U \times V \times W_{iy}$
 203 **end for**
 204 **end for**
 205 **return** W_{ix} and W_{iy}

208 4 EXPERIMENT AND DISCUSSION

211 4.1 SAMPLE PREPARATION

212
 213 This paper utilizes patterns from the MNIST dataset, each of which contains 784 nodes (28×28),
 214 and the character script dataset, which includes regular script (53×40) and seal script (40×40). The
 215 goal of this exploration is to associate paired digit patterns and to associate regular script with its
 corresponding seal script. All patterns are converted into bipolar form.

216 **Algorithm 2** Bidirectional Back-Propagation with OWM and GPA Regularizes

217 **Input:** Samples X, Y, N(Number of Layers) ,and the Epoch

218 **Output:** weight matrix W_i

219 **Initialization:** Initialize the orthogonal weight matrices W_i . For convenience, the two ends of the

220 BAM are referred to as follows: the input end X is called A , and the input end Y is called B . The

221 symbol \times indicates matrix multiplication in this algorithm.

222 **for** index $\leftarrow 1$ to Epoch **do**

223 Train the BAM using the loss value from both A and B end

224 While calculating the value of OWM and GPA to regularize the training process

225 $\hat{B} = A_FORWARD_B(X, \text{layer}=N)$

226 $\hat{A} = B_FORWARD_A(Y, \text{layer}=0)$

227 $loss_A = \text{MSE}(\hat{A}, A)$

228 $loss_B = \text{MSE}(\hat{B}, B)$

229 $grad_A = \text{GRADIENT}(loss_B, A)$

230 $grad_B = \text{GRADIENT}(loss_A, B)$

231 $ALIGN = \text{CosSim}(grad_A, A) + \text{CosSim}(grad_B, B)$

232 $ORTH = \sum_{i=0}^n \text{MEAN}(W_i \times W_i^T - I)$

233 $LOSS = loss_A + loss_B + \lambda_{align} ALIGN + \lambda_{orth} ORTH$

234 Back-propagation the LOSS to Update weight matrix.

235 **end for**

236 **return** W

237

238 4.2 EXPERIMENT CONFIGURATION

239

240 In training BAM, B-BP uses the Adam optimizer with a learning rate set to 0.0001. The output logits

241 from the A end and the B end are used to compute the loss value, and the loss values from both

242 ends are combined to calculate the gradient of the weight matrix. In contrast, when using B-SRA

243 to train BAM, hyperparameters are not required, but the weight matrix is initialized orthogonally.

244 Additionally, for discrete BAM, a sign function is applied to the output during the inference, and

245 the result is compared against the corresponding bipolar pattern to determine whether the BAM can

246 retrieve all patterns correctly iteratively.

247

248 4.3 EXPLORING THE ROBUSTNESS OF BAM TRAINED BY B-SRA AND B-BP

249 Figures 1 present initial experiments evaluating the robustness of BAM trained solely with B-SRA and

250 B-BP. In Figure 1(a), we train BAM to associate 20 digit patterns with another 20 digit patterns. When

251 half of the query pattern is masked, the BAM trained by B-BP fails to retrieve the correct associations,

252 demonstrating multiple retrieval errors. In contrast, the BAM trained by B-SRA successfully recalls

253 the target patterns without any error bits, highlighting its larger basin of attraction under partial

254 masking. Similarly, when GN (mean = 0, variance = 1) is added to the query inputs (Figure 1(b)),

255 only the BAM trained by B-SRA retains retrieval accuracy, while the BAM trained by B-BP degrades

256 significantly.

257 Figure 1(c) and 1(d) further investigates adversarial robustness using FGSM attacks. The BAM

258 trained by B-BP fails completely at even mild perturbation levels ($\epsilon = 0.2$), whereas the BAM trained

259 by B-SRA accurately recalls the target patterns even under strong attacks ($\epsilon = 0.9$). These results

260 consistently show that, in the absence of regularization, the B-BP algorithm fails to produce robust

261 associative memories. In contrast, the BAM trained by B-SRA, by design, produces models that are

262 naturally resilient to noise and adversarial perturbations.

263 These findings motivate the following section, where we introduce regularization techniques into the

264 B-BP framework. By enforcing weight orthogonality and gradient-pattern alignment, we show that

265 B-BP can be enhanced to achieve or exceed the robustness levels of BAM trained by B-SRA.

266

267 4.3.1 ROBUSTNESS ANALYSIS FOR BAM TRAINED BY B-SRA

268

269 As discussed in Section 4.3, the BAM trained by B-SRA is robust to corrupted or noisy pattern

inputs and resilient under adversarial attacks. Through multiple experiments and careful analysis, we

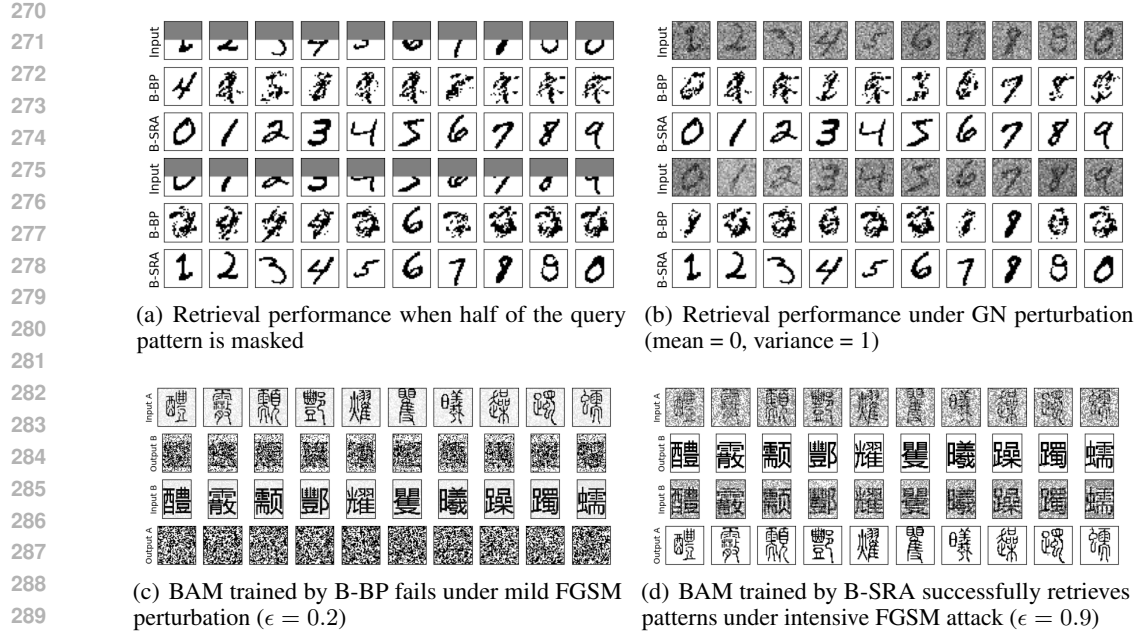


Figure 1: Retrieval performance of BAM trained by B-BP and B-SRA under masking and GN

conclude that two key factors significantly contribute to this robustness: (i) the orthogonality of the weight matrix and (ii) the alignment of the gradient and patterns.

Assuming f is a nonlinear activation function, such as tanh or ReLU, used in the BAM, it typically serves to squash or suppress the magnitude of signals. The robustness provided by the orthogonal matrix can be understood through the lens of a condition number analysis. For an orthogonal matrix, which preserves the norm and has a condition number of 1, the following Equation 8 always holds.

$$\|f[W(x + \delta)]\|_F \leq \|W(x + \delta)\|_F = \|Wx + W\delta\|_F = \|x + \delta\|_F \leq \|x\|_F + \|\delta\|_F \quad (8)$$

This ensures that the signal can pass through the network without being distorted, and at the same time, it guarantees that noise is not amplified as the signal propagates from end a to end b, or vice versa.

In terms of the GPA, for a well-trained deep BAM with non-linear activation where the gradient aligns with the patterns, $\frac{\partial \mathcal{L}}{\partial X} = \alpha X$. From the perspective of the loss landscape, it is straightforward to understand that the loss increases most significantly along the direction of X. In other words, the loss landscape is relatively flat in directions perpendicular to X. Typically, noise that is perpendicular to the pattern X is more harmful than noise that is aligned with X, since the latter is inherently suppressed in deep learning models due to activation function damping or cancellation by normalization layers. Therefore, combining GPA with OWM can significantly enhance the robustness of the BAM.

Therefore, to enhance the robustness of BAM trained via B-BP, it is essential to incorporate both the OWM and GPA regularizers into the final objective function. In Section 4.3.2, we analyze how each component contributes to the resilience of BAM.

324 4.3.2 ABLATION STUDY ON REGULARIZATION TECHNIQUES FOR BAM ROBUSTNESS
325
326
327328 Table 1: Robustness-Related Metrics: GPA and OWM
329

Strategy	GPA(A)	GPA(B)	OWM(A)	OWM(B)
SRA	-0.96 ± 0.001	0.561 ± 0.001	0.0 ± 0.0	0.0 ± 0.0
ORTH	-0.31 ± 0.003	0.989 ± 0.0	18.796 ± 0.705	11.159 ± 0.253
SAME	0.99 ± 0.001	0.99 ± 0.0	37.442 ± 0.21	16.872 ± 0.076
DIFF	-0.979 ± 0.003	0.969 ± 0.006	10.89 ± 1.0	7.268 ± 0.338
ALIGN	0.99 ± 0.0	0.999 ± 0.0	695.247 ± 1.997	524.527 ± 1.068
BP	-0.09 ± 0.007	0.999 ± 0.0	684.59 ± 1.236	526.135 ± 0.799

335 In this section, we associate 50 pairs of regular and seal script patterns to perform an ablation
336 study and assess the individual contribution of each regularization technique to BAM’s robust-
337 ness. The following abbreviations are used throughout the paper: SRA denotes the Subspace
338 Rotation Algorithm; ORTH refers to BAM trained with the OWM regularizer; SAME applies both
339 OWM and GPA with aligned directions; DIFF uses both regularizers but with opposing alignment;
340 ALIGN applies only GPA without OWM; and BP denotes standard Bidirectional Backpropagation.

341 Table 2: Robustness of BAM Trained with Different Strategies Under Adversarial Attacks^[1]
342

Attackers ^[2]	Strategies	Input A ^[3]	Output B ^[3]	Input B ^[3]	Output A ^[3]
GN	SRA	12.27 ± 0.058	0.674 ± 0.036	12.243 ± 0.057	0.196 ± 0.036
	ORTH	12.26 ± 0.057	0.06 ± 0.025	12.255 ± 0.048	0.038 ± 0.002
	SAME	12.217 ± 0.046	0.42 ± 0.099	12.25 ± 0.036	0.066 ± 0.015
	DIFF	12.279 ± 0.063	1.336 ± 0.012	12.231 ± 0.05	1.311 ± 0.013
	ALIGN	12.268 ± 0.055	1.95 ± 0.007	12.251 ± 0.033	1.943 ± 0.004
	BP	12.239 ± 0.052	1.964 ± 0.007	12.252 ± 0.052	1.958 ± 0.006
FGSM	SRA	1.21 ± 0.0	0.0 ± 0.0	1.21 ± 0.0	0.004 ± 0.0
	ORTH	1.21 ± 0.0	0.006 ± 0.003	1.21 ± 0.0	0.037 ± 0.001
	SAME	1.21 ± 0.0	0.005 ± 0.004	1.21 ± 0.0	0.04 ± 0.002
	DIFF	1.21 ± 0.0	0.167 ± 0.012	1.21 ± 0.0	0.0 ± 0.0
	ALIGN	1.21 ± 0.0	1.867 ± 0.013	1.21 ± 0.0	1.882 ± 0.007
	BP	1.21 ± 0.0	1.903 ± 0.02	1.21 ± 0.0	1.899 ± 0.01
FFGSM	SRA	1.387 ± 0.004	0.0 ± 0.0	2.184 ± 0.007	0.004 ± 0.0
	ORTH	1.388 ± 0.004	0.004 ± 0.001	2.187 ± 0.006	0.037 ± 0.001
	SAME	1.388 ± 0.003	0.005 ± 0.004	2.18 ± 0.004	0.041 ± 0.005
	DIFF	1.387 ± 0.004	0.672 ± 0.042	2.182 ± 0.006	0.985 ± 0.022
	ALIGN	1.386 ± 0.006	1.894 ± 0.008	2.183 ± 0.006	1.921 ± 0.004
	BP	1.388 ± 0.005	1.924 ± 0.012	2.184 ± 0.005	1.935 ± 0.014
PGD	SRA	1.648 ± 0.002	0.387 ± 0.051	2.042 ± 0.003	0.004 ± 0.0
	ORTH	1.645 ± 0.005	0.011 ± 0.006	2.042 ± 0.003	0.038 ± 0.001
	SAME	1.645 ± 0.005	0.168 ± 0.044	2.041 ± 0.004	0.04 ± 0.002
	DIFF	1.649 ± 0.004	1.398 ± 0.025	2.042 ± 0.004	0.581 ± 0.023
	ALIGN	1.649 ± 0.002	1.951 ± 0.008	2.041 ± 0.003	1.908 ± 0.006
	BP	1.646 ± 0.006	1.964 ± 0.037	2.04 ± 0.003	1.925 ± 0.006

¹ Notes apply to Table 1, 2, 3, and 4.

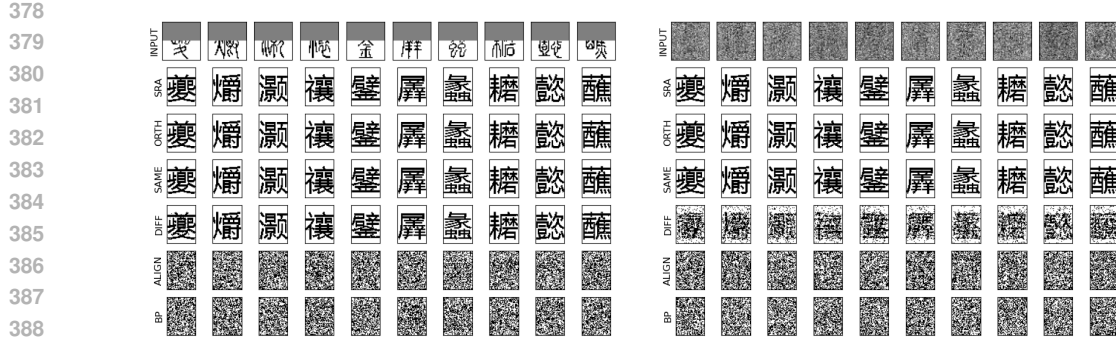
² All attackers of the same type are configured with the same parameters across experiments for fair comparison.

³ Input A and Input B columns report the mean squared error (MSE) of the adversarial noise added to the respective inputs. Output B and Output A columns show the MSE of the retrieved patterns under perturbation. **Lower output values indicate better robustness.**

366 As shown in Table 1, the BAM trained by B-SRA achieves optimal values for OWM regularization at
367 both ends, and reasonably good GPA (-0.96 at the a end and 0.561 at the b end). In contrast, while it is
368 challenging for the BAM trained by B-BP to achieve optimal OWM values, it can attain near-optimal
369 GPA values at b end (0.999), even without any regularizers.

370 It is also observed that the DIFF strategy achieves better OWM values than the SAME strategy (e.g.,
371 10.89 vs. 37.44 at the a end), but subsequent evaluations show that BAM trained with SAME or
372 ORTH demonstrates greater robustness than DIFF, even when the latter has superior OWM metrics,
373 as shown in Figure 2. This discrepancy suggests that negative GPA values, such as the -0.979 seen in
374 DIFF, may contribute to the vulnerability of the BAM under corruption or noise.

375 Furthermore, the ALIGN strategy achieves nearly perfect GPA at both ends but suffers from extremely
376 high OWM (e.g., over 695 at a end), which significantly reduces its robustness, as shown in Figure 2.
377 These findings indicate that both GPA and OWM are critical and complementary indicators of BAM’s
robustness. Overemphasis on one while neglecting the other can compromise system reliability.



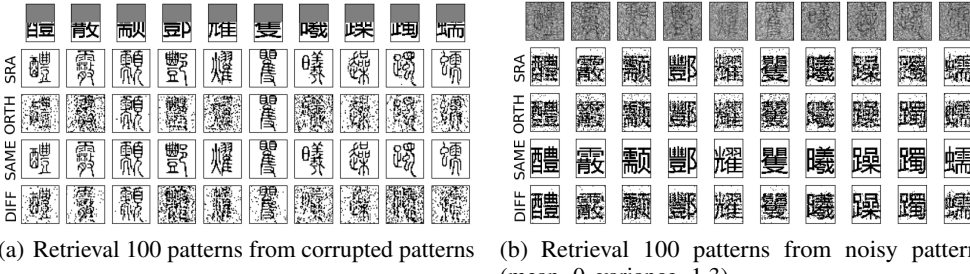
378
379
380
381
382
383
384
385
386
387
388
389
390
391
392
393
394
395
396
397
398
399
400
401
402
403
404
405
406
407
408
409
410
411
412
413
414
415
416
417
418
419
420
421
422
423
424
425
426
427
428
429
430
431

(a) Retrieval performance of models when half of the query pattern is masked (b) Retrieval performance of models under GN perturbation (mean=0, variance=2)

Figure 2: Comparison of retrieval performance for different models when query patterns are corrupted or noisy

To further evaluate the robustness of BAM trained with different strategies, several adversarial attack approaches are applied, including GN, FGSM, FFGSM, and PGD. As shown in Table 2, under strong GN perturbation, the ORTH strategy performs the best, followed by SAME and then SRA. However, for FGSM and FFGSM attackers, SRA achieves the best performance, while ORTH and SAME perform similarly without significant difference. Under the PGD attacker, SRA is able to retrieve patterns at the b-end with lower error, whereas ORTH and SAME yield better results at the a-end. These results suggest that SRA, ORTH, and SAME strategies are comparably effective in resisting various types of adversarial attacks, each showing strengths under different conditions.

4.4 CASE STUDY: BIDIRECTIONALLY ASSOCIATING 100 PAIRS OF REGULAR AND SEAL SCRIPT



(a) Retrieval 100 patterns from corrupted patterns (b) Retrieval 100 patterns from noisy patterns (mean=0, variance=1.3)

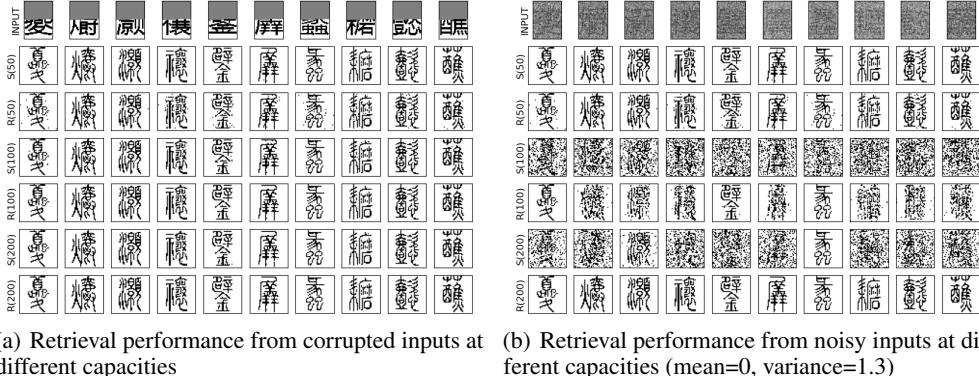
Figure 3: Retrieval performance of BAM trained with different strategies on 100 script pattern pairs

To further evaluate the robustness of BAM trained with different strategies, we conduct an experiment where the BAM is tasked with associating 100 pairs of regular and seal script characters. A quick inspection of Figure 3 shows that when 50% of the input pattern is masked, the SRA and SAME strategies can retrieve the correct patterns with almost no error. Under noisy input conditions (mean = 0, variance = 1.2), the SAME strategy achieves the best performance among all methods. Table 3 further validates these observations by quantifying model robustness under a variety of adversarial attacks. The SAME strategy performs the best under GN, FGSM, and BIM attacks, demonstrating significant advantages in both the A and B directions. For the FFGSM attack, SAME slightly underperforms compared to SRA at the B-end. Under PGD attacks, SAME also performs slightly worse than SRA at the A-end. In conclusion, the SAME strategy consistently performs well across a range of challenging conditions and exhibits the most balanced and reliable robustness profile. These findings suggest that SAME has

432 strong potential to serve as an optimal training strategy for enhancing the robustness of BAM.
 433

434 Table 3: Robustness of BAM Trained with Different Strategies on 100 Script Pattern Pairs
 435

Attackers	Strategies	Input A	Output B	Input B	Output A
GN	SRA	1.44 ± 0.004	0.407 ± 0.006	1.44 ± 0.004	0.097 ± 0.007
	ORTH	1.442 ± 0.004	0.557 ± 0.023	1.44 ± 0.005	0.574 ± 0.04
	SAME	1.441 ± 0.004	0.023 ± 0.014	1.44 ± 0.003	0.019 ± 0.011
	DIFF	1.444 ± 0.006	0.354 ± 0.013	1.44 ± 0.004	0.319 ± 0.041
FGSM	SRA	1.21 ± 0.0	2.057 ± 0.008	1.21 ± 0.0	0.564 ± 0.011
	ORTH	1.21 ± 0.0	1.468 ± 0.065	1.21 ± 0.0	0.101 ± 0.024
	SAME	1.21 ± 0.0	0.0 ± 0.0	1.21 ± 0.0	0.0 ± 0.0
	DIFF	1.21 ± 0.0	1.663 ± 0.029	1.21 ± 0.0	0.0 ± 0.0
FFGSM	SRA	0.575 ± 0.001	0.05 ± 0.003	0.95 ± 0.0	1.81 ± 0.006
	ORTH	0.591 ± 0.001	0.669 ± 0.047	0.93 ± 0.002	1.373 ± 0.063
	SAME	0.58 ± 0.006	0.075 ± 0.038	0.899 ± 0.007	0.115 ± 0.076
	DIFF	0.57 ± 0.001	0.414 ± 0.015	0.893 ± 0.001	1.774 ± 0.018
BIM	SRA	0.94 ± 0.001	1.842 ± 0.004	0.998 ± 0.0	0.371 ± 0.009
	ORTH	0.804 ± 0.004	1.937 ± 0.202	0.976 ± 0.002	0.187 ± 0.042
	SAME	0.755 ± 0.006	0.062 ± 0.066	0.975 ± 0.004	0.0 ± 0.0
	DIFF	0.845 ± 0.002	1.534 ± 0.017	0.947 ± 0.003	0.231 ± 0.102
PGD	SRA	0.885 ± 0.0	1.647 ± 0.004	0.984 ± 0.0	0.113 ± 0.006
	ORTH	0.822 ± 0.002	2.304 ± 0.017	0.937 ± 0.002	1.055 ± 0.058
	SAME	0.782 ± 0.006	1.258 ± 0.2	0.921 ± 0.008	0.125 ± 0.062
	DIFF	0.823 ± 0.002	1.383 ± 0.012	0.897 ± 0.005	0.773 ± 0.058

450
 451 4.5 EVALUATING THE RELATIONSHIP BETWEEN CAPACITY AND ROBUSTNESS IN BAM
 452
 453468 Figure 4: Effect of memory capacity on retrieval performance of BAM trained with different strategies
 469

470 In this section, we analyze the relationship between memory capacity and the robustness of BAM
 471 trained with SRA and SAME by comparing the results presented in Table 4 and Figure 4(a) and
 472 4(b). The BAM models are evaluated under varying memory capacities—associating 50, 100, and
 473 200 pattern pairs—across different adversarial attackers. It is important to note that for storing 50
 474 and 100 pattern pairs, a 3-layer BAM is used, whereas a 5-layer BAM is employed for the 200-pair
 475 configuration.

476 Figure 4(a) shows that, under 50% masking, all models are able to retrieve the correct patterns with
 477 relatively low bit errors. However, Figure 4(b) reveals that the BAM trained with SAME to store 200
 478 pairs of patterns (denoted as R(200)) achieves the best performance under noisy input conditions.
 479 This indicates that the deeper BAM architecture may contribute to the improved robustness observed
 480 under the SAME strategy.

481 It is observed that for the BAM trained with SRA, retrieval performance gradually degrades
 482 with increasing capacity, as shown in Table 4. In contrast, the BAM trained with the SAME
 483 strategy to store 200 pairs of patterns achieves the best performance among all models, and
 484 the BAM trained with SAME to store 50 pairs performs only slightly worse. This suggests
 485 that increasing the number of layers may allow the SAME strategy to fully realize its poten-

486 trial, yielding the best possible robustness—even as the number of memorized patterns increases.
 487

488 Table 4: Comparative Study of BAM Robustness Across Memory Sizes (50, 100, 200 Pairs)

490 Attackers	491 Strategies	492 Input A	493 Output B	494 Input B	495 Output A
GN	SRA(50)	2.25 ± 0.013	0.46 ± 0.345	2.251 ± 0.009	0.192 ± 0.26
	SAME(50)	2.253 ± 0.012	0.057 ± 0.086	2.247 ± 0.008	0.08 ± 0.098
	SRA(100)	2.247 ± 0.011	0.455 ± 0.344	2.252 ± 0.008	0.195 ± 0.266
	SAME(100)	2.253 ± 0.01	0.073 ± 0.1	2.251 ± 0.008	0.083 ± 0.098
	SRA(200)	2.252 ± 0.013	0.493 ± 0.334	2.251 ± 0.008	0.205 ± 0.264
	SAME(200)	2.253 ± 0.012	0.061 ± 0.088	2.246 ± 0.008	0.082 ± 0.101
FGSM	SRA(50)	1.21 ± 0.0	1.227 ± 0.717	1.21 ± 0.0	0.743 ± 0.71
	SAME(50)	1.21 ± 0.0	0.002 ± 0.004	1.21 ± 0.0	0.013 ± 0.019
	SRA(100)	1.21 ± 0.0	1.219 ± 0.737	1.21 ± 0.0	0.739 ± 0.711
	SAME(100)	1.21 ± 0.0	0.001 ± 0.001	1.21 ± 0.0	0.013 ± 0.019
	SRA(200)	1.21 ± 0.0	1.293 ± 0.697	1.21 ± 0.0	0.796 ± 0.706
	SAME(200)	1.21 ± 0.0	0.002 ± 0.004	1.21 ± 0.0	0.011 ± 0.018
FFGSM	SRA(50)	0.565 ± 0.036	0.02 ± 0.019	0.962 ± 0.017	1.913 ± 0.075
	SAME(50)	0.528 ± 0.036	0.023 ± 0.03	0.916 ± 0.017	0.038 ± 0.043
	SRA(100)	0.565 ± 0.036	0.021 ± 0.02	0.962 ± 0.017	1.91 ± 0.079
	SAME(100)	0.528 ± 0.037	0.034 ± 0.044	0.916 ± 0.017	0.056 ± 0.07
	SRA(200)	0.568 ± 0.035	0.021 ± 0.019	0.961 ± 0.017	1.907 ± 0.074
	SAME(200)	0.53 ± 0.036	0.025 ± 0.031	0.915 ± 0.017	0.037 ± 0.045
BIM	SRA(50)	0.856 ± 0.081	1.668 ± 0.197	0.957 ± 0.053	0.777 ± 0.933
	SAME(50)	0.652 ± 0.077	0.694 ± 0.452	0.875 ± 0.161	0.255 ± 0.333
	SRA(100)	0.856 ± 0.082	1.666 ± 0.201	0.957 ± 0.053	0.777 ± 0.936
	SAME(100)	0.653 ± 0.078	0.68 ± 0.454	0.875 ± 0.159	0.253 ± 0.33
	SRA(200)	0.864 ± 0.078	1.688 ± 0.189	0.954 ± 0.054	0.833 ± 0.942
	SAME(200)	0.657 ± 0.077	0.679 ± 0.465	0.866 ± 0.163	0.27 ± 0.34
PGD	SRA(50)	0.843 ± 0.045	1.58 ± 0.116	0.936 ± 0.06	0.609 ± 0.819
	SAME(50)	0.711 ± 0.051	1.205 ± 0.161	0.859 ± 0.147	0.29 ± 0.302
	SRA(100)	0.843 ± 0.045	1.583 ± 0.117	0.936 ± 0.059	0.608 ± 0.824
	SAME(100)	0.71 ± 0.052	1.228 ± 0.153	0.859 ± 0.146	0.297 ± 0.296
	SRA(200)	0.848 ± 0.043	1.592 ± 0.112	0.933 ± 0.061	0.653 ± 0.831
	SAME(200)	0.714 ± 0.052	1.211 ± 0.165	0.849 ± 0.148	0.307 ± 0.305

511 5 CONCLUSION AND FUTURE STUDY

512 This paper introduces a novel gradient-free training method, B-SRA, for training BAM. Experimental
 513 results show that BAM trained with B-SRA demonstrates strong robustness against adversarial attacks.
 514 Motivated by this phenomenon, we identify two key factors that contribute to the robustness of BAM:
 515 OWM and GPA. Based on these insights, we design two regularization strategies for B-BP to enhance
 516 the resilience of BAM significantly.

517 Through extensive experiments, including pattern association tasks with digits and Chinese character
 518 scripts, we demonstrate that BAM trained with B-SRA achieves superior robustness compared
 519 to traditional B-BP. Furthermore, the inclusion of GPA and OWM regularizers in B-BP leads
 520 to significant gains in adversarial resilience. Among the training strategies studied, the SAME
 521 strategy—using OWM and GPA in the same direction—consistently achieves the best performance,
 522 especially in deeper BAM architectures with larger memory capacities.

523 For future work, we aim to extend our findings from BAM to broader deep learning frameworks.
 524 Since BAM shares similarities with the attention mechanism and the architecture of modern Hopfield
 525 networks, we plan to incorporate our insights into Transformer and Hopfield-based architectures to
 526 develop more robust models. We would also like to develop adversarial attackers specifically designed
 527 to target BAM. Since BAM is a purely recurrent neural network, it is fundamentally different from
 528 standard feed-forward deep learning models. As such, existing gradient-based attacks may not be
 529 suitable for effectively evaluating the vulnerabilities of BAM.

533 REFERENCES

- 534 Maria Elena Acevedo-Mosqueda, Cornelio Yanez-Marquez, and Marco Antonio Acevedo-Mosqueda.
 535 Bidirectional associative memories: Different approaches. *ACM Computing Surveys (CSUR)*, 45
 536 (2):1–30, 2013.
- 537 Olaoluwa Adigun and Bart Kosko. Bidirectional backpropagation. *IEEE Transactions on Systems,
 538 Man, and Cybernetics: Systems*, 50(5):1982–1994, 2019.

- 540 Chunhua Feng and Rejean Plamondon. Stability analysis of bidirectional associative memory
 541 networks with time delays. *IEEE Transactions on Neural Networks*, 14(6):1560–1565, 2003.
 542
- 543 C Lee Giles and Tom Maxwell. Learning, invariance, and generalization in high-order neural
 544 networks. *Applied optics*, 26(23):4972–4978, 1987.
- 545 Ian J Goodfellow, Jonathon Shlens, and Christian Szegedy. Explaining and harnessing adversarial
 546 examples. *arXiv preprint arXiv:1412.6572*, 2014.
 547
- 548 Mohamad H Hassoun and Paul B Watt. Associative memory networks. In *Handbook of neural
 549 computation*, pp. C1–3. CRC Press, 2020.
- 550 Kai-Chieh Hsu, Haimin Hu, and Jaime F Fisac. The safety filter: A unified view of safety-critical
 551 control in autonomous systems. *Annual Review of Control, Robotics, and Autonomous Systems*, 7,
 552 2023.
- 553 Geethan Karunaratne, Manuel Schmuck, Manuel Le Gallo, Giovanni Cherubini, Luca Benini, Abu
 554 Sebastian, and Abbas Rahimi. Robust high-dimensional memory-augmented neural networks.
 555 *Nature communications*, 12(1):2468, 2021.
- 556 Bart Kosko. Bidirectional associative memories: unsupervised Hebbian learning to bidirectional
 557 backpropagation. *IEEE Transactions on Systems, Man, and Cybernetics: Systems*, 51(1):103–115,
 558 2021.
- 559 Dmitry Krotov and John J Hopfield. Dense associative memory for pattern recognition. *Advances in
 560 neural information processing systems*, 29, 2016.
- 561 Alexey Kurakin, Ian J Goodfellow, and Samy Bengio. Adversarial examples in the physical world.
 562 In *Artificial intelligence safety and security*, pp. 99–112. Chapman and Hall/CRC, 2018.
- 563 Chi-Sing Leung, Lai-Wan Chan, and Edmund Lai. Stability, capacity, and statistical dynamics
 564 of second-order bidirectional associative memory. *IEEE Transactions on Systems, Man, and
 565 Cybernetics*, 25(10):1414–1424, 1995.
- 566 Ci Lin, Tet Yeap, and Iluju Kiringa. On the basin of attraction and capacity of restricted hopfield
 567 network as an auto-associative memory. In *2023 International Conference on Cyber-Enabled
 568 Distributed Computing and Knowledge Discovery (CyberC)*, pp. 146–154, 2023. doi: 10.1109/
 569 CyberC58899.2023.00033.
- 570 Ci Lin, Tet Yeap, and Iluju Kiringa. Subspace Rotation Algorithm for Training Restricted Hopfield
 571 Network. *36th IEEE International Conference on Tools with Artificial Intelligence (ICTAI 2024)*,
 572 2024.
- 573 Ci Lin, Tet Yeap, Iluju Kiringa, and Biwei Zhang. Restricted Hopfield Networks are Robust to
 574 Adversarial Attack. *Authorea Preprints*, 2025.
- 575 Aleksander Madry, Aleksandar Makelov, Ludwig Schmidt, Dimitris Tsipras, and Adrian Vladu.
 576 Towards deep learning models resistant to adversarial attacks. *arXiv preprint arXiv:1706.06083*,
 577 2017.
- 578 Taofiq K Paraiso, Thomas Roger, Davide G Marangon, Innocenzo De Marco, Mirko Sanzaro, Robert I
 579 Woodward, James F Dynes, Zhiliang Yuan, and Andrew J Shields. A photonic integrated quantum
 580 secure communication system. *Nature photonics*, 15(11):850–856, 2021.
- 581 Hubert Ramsauer, Bernhard Schäfl, Johannes Lehner, Philipp Seidl, Michael Widrich, Lukas Gruber,
 582 Markus Holzleitner, Thomas Adler, David Kreil, Michael K Kopp, et al. Hopfield Networks is All
 583 You Need. In *International Conference on Learning Representations*, 2022.
- 584 Frank Rosenblatt et al. *Principles of neurodynamics: Perceptrons and the theory of brain mechanisms*,
 585 volume 55. Spartan books Washington, DC, 1962.
- 586 Peter H Schönemann. A generalized solution of the orthogonal procrustes problem. *Psychometrika*,
 587 31(1):1–10, 1966.

- 594 Anthony Strock, Xavier Hinaut, and Nicolas P Rougier. A robust model of gated working memory.
595 *Neural Computation*, 32(1):153–181, 2020.
596
- 597 Eric Wong, Leslie Rice, and J Zico Kolter. Fast is better than free: Revisiting adversarial training.
598 *arXiv preprint arXiv:2001.03994*, 2020.
- 599 Houding Zhang and Zexian Yang. Biometric Authentication and Correlation Analysis Based on
600 CNN-SRU Hybrid Neural Network Model. *Computational Intelligence and Neuroscience*, 2023
601 (1):8389193, 2023.
- 602
- 603 Yutong Zhang and Zhigang Zeng. Brain-inspired model and neuromorphic circuit implementation for
604 feature-affective associative memory network. *IEEE Transactions on Cognitive and Developmental
605 Systems*, 16(5):1707–1721, 2023.
- 606
- 607
- 608
- 609
- 610
- 611
- 612
- 613
- 614
- 615
- 616
- 617
- 618
- 619
- 620
- 621
- 622
- 623
- 624
- 625
- 626
- 627
- 628
- 629
- 630
- 631
- 632
- 633
- 634
- 635
- 636
- 637
- 638
- 639
- 640
- 641
- 642
- 643
- 644
- 645
- 646
- 647

648 TABLE OF CONTENTS
649

650	1	Introduction	1
651	1.1	Motivation and Contribution	2
652	1.2	Organization	2
653			
654			
655	2	Bidirectional Associative Memory	2
656	2.1	Stability Analysis	3
657			
658			
659	3	Bidirectional Subspace Rotation Algorithm	3
660	3.1	Mathematical Mechanism for Bidirectional Subspace Rotation Algorithm	3
661	3.2	Pseudo-code for B-SRA and B-BP with two regularizers	4
662			
663			
664	4	Experiment and Discussion	4
665	4.1	Sample Preparation	4
666	4.2	Experiment Configuration	5
667	4.3	Exploring the Robustness of BAM Trained by B-SRA and B-BP	5
668	4.4	Case Study: Bidirectionally Associating 100 Pairs of Regular and Seal Script	8
669	4.5	Evaluating the Relationship Between Capacity and Robustness in BAM	9
670			
671			
672			
673	5	Conclusion and Future Study	10
674			
675			
676	A	Bidirectional Backpropagation Algorithm	13
677	A.1	Regularization Strategies for Enhancing B-BP Training	14
678			
679	B	Mathematical Mechanism for Bidirectional Subspace Rotation Algorithm	15
680			
681	C	Adversarial Attack Algorithms	16
682			
683	D	Extended Experimental Results on BAM Robustness	16
684	D.1	Initial Experiment on B-SRA and B-BP	16
685	D.2	Ablation Study for Individual Regularization	18
686	D.3	Case Study: Association of 100 Pairs of Script Patterns	18
687			
688			
689			
690	A	BIDIRECTIONAL BACKPROPAGATION ALGORITHM	
691			
692			
693	B-BP is an extension of traditional backpropagation, designed to optimize both the forward and backward mappings of a neural network (Adigun & Kosko, 2019).		
694			
695	The forward pass maps an input x_i to an output y_i using a function $f(x; \Theta)$, parameterized by		
696	$\Theta = \{\theta_0, \theta_1, \dots, \theta_n\}$. For a dataset of N samples, the forward mapping is represented as in		
697	Equation 9.		
698			
699	$y_i = f(x_i; \Theta), \quad i = 1, 2, \dots, N$		(9)
700			

701 The forward error E_f is defined as the sum of losses over all samples in the dataset, as shown in
Equation 10.

702
703
704
705
706
707
708

$$E_f[\Theta] = \frac{1}{N} \sum_{i=1}^N \mathcal{L}_f(f(x_i; \Theta), y_i^{\text{true}}) \quad (10)$$

where \mathcal{L}_f is the forward loss function, which can take various forms (e.g., mean squared error, cross-entropy) and y_i^{true} is the ground truth output for input x_i .

The backward pass approximates the reconstruction of the input x_i from the output y_i using the same parameters Θ . The backward mapping is represented as in Equation 11.

711
712
713
714
715
716
717
718
719

$$\hat{x}_i = g(y_i; \Theta), \quad i = 1, 2, \dots, N \quad (11)$$

The backward error E_b is defined similarly as the sum of losses over all samples in the dataset, as shown in Equation 12.

720
721
722
723
724
725
726
727
728
729
730
731
732

$$E_b[\Theta] = \frac{1}{N} \sum_{i=1}^N \mathcal{L}_b(g(y_i; \Theta), x_i^{\text{true}}) \quad (12)$$

where \mathcal{L}_b is the backward loss function, which can also vary depending on the task. x_i^{true} is the original input corresponding to the output y_i .

The total error to be minimized is the sum of the forward and backward errors, as shown in Equation 13.

733
734
735
736
737
738
739
740
741
742
743
744
745
746
747
748
749
750
751
752
753
754
755

$$E[\Theta] = E_f[\Theta] + E_b[\Theta] \quad (13)$$

The gradients of the total error with respect to each parameter θ_k are calculated, as shown in Equation 14.

$$\Delta\Theta = -\eta \left(\frac{\partial E_f[\Theta]}{\partial \Theta} + \frac{\partial E_b[\Theta]}{\partial \Theta} \right) \quad (14)$$

Parameters Θ are iteratively updated using these gradients until the neural network converges.

A.1 REGULARIZATION STRATEGIES FOR ENHANCING B-BP TRAINING

To improve the robustness of the Bidirectional Backpropagation (B-BP) algorithm, we introduce two regularization terms: orthogonal weight matrix (OWM) regularization and gradient-pattern alignment (GPA) regularization. These are applied in the context of a neural network defined abstractly as $Y = f(X)$, with training based on the mean squared error loss:

$$\mathcal{L}_{\text{reconstruction}} = \|\hat{Y} - Y\|^2$$

This regularizer penalizes deviation from orthogonality in the weight matrix W , encouraging well-conditioned mappings that preserve input signal magnitudes:

$$\mathcal{L}_{\text{ortho}} = \lambda_{\text{ortho}} \cdot \|W^\top W - I\|_F^2$$

where $\|\cdot\|_F$ is the Frobenius norm, I is the identity matrix, and λ_{ortho} is a coefficient controlling the regularization strength.

This regularizer promotes alignment between the input pattern X and the gradient of the loss with respect to X . The alignment is evaluated using cosine similarity:

$$\mathcal{L}_{\text{align}} = \lambda_{\text{align}} \cdot (1 - \cos \theta), \quad \text{where} \quad \cos \theta = \frac{\langle \nabla_X \mathcal{L}, X \rangle}{\|\nabla_X \mathcal{L}\| \cdot \|X\|}$$

Here, $\nabla_X \mathcal{L}$ is the gradient of the loss with respect to input X , and λ_{align} balances the contribution of this term.

756 The full training objective becomes:
 757

$$\mathcal{L}_{\text{total}} = \mathcal{L}_{\text{reconstruction}} + \mathcal{L}_{\text{ortho}} + \mathcal{L}_{\text{align}}$$

759
 760 **B MATHEMATICAL MECHANISM FOR BIDIRECTIONAL SUBSPACE ROTATION**
 761 **ALGORITHM**
 762

763 In analyzing the mathematical mechanism of BAM, let us start with the most fundamental and original
 764 BAM, which consists of a Hopfield Neural Network (HNN), as shown in Equation 15.

$$\begin{cases} Y = WX \\ X = W^T Y \end{cases} \quad (15)$$

765 For randomly initialized \hat{W} , the outputs are \hat{Y} and \hat{X} respectively. Now, the question becomes how
 766 can we rotate the \hat{W} to make the distance between Y and \hat{Y} and X and \hat{X} minimum. Then we need
 767 to optimize the Equation 16.

$$\min_{Q^T Q = I_p} \|Y - \hat{Y}Q\|_F + \|X - \hat{X}Q^T\|_F \quad (16)$$

774 If $Q \in \mathbb{R}^{p \times p}$ is orthogonal, we get Equation 17.
 775

$$\begin{aligned} \|Y - \hat{Y}Q\|_F^2 &= \sum_{k=1}^p \|Y(:, k) - \hat{Y}Q(:, k)\|_F^2 \\ &= \sum_{k=1}^p (\|Y(:, k)\|_F^2 + \|\hat{Y}Q(:, k)\|_F^2 \\ &\quad - 2Q(:, k)^T \hat{Y}^T Y(:, k)) \\ &= \|Y\|_F^2 + \|\hat{Y}\|_F^2 - 2 \sum_{k=1}^p [Q^T \hat{Y}^T Y]_{kk} \\ &= \|Y\|_F^2 + \|\hat{Y}\|_F^2 - 2 \text{tr}(Q^T (\hat{Y}^T Y)) \end{aligned} \quad (17)$$

787 Similarly, we could obtain the Equation 18.
 788

$$\|X - \hat{X}Q^T\|_F^2 = \|X\|_F^2 + \|\hat{X}\|_F^2 - 2 \text{tr}((\hat{X}^T X Q)) \quad (18)$$

790 Now, Optimizing the Equation 7 is equivalent to optimizing Equation 19.
 791

$$\max_{Q^T Q = I_p} \text{tr}(Q^T \hat{Y}^T Y) + \text{tr}(\hat{X}^T X Q) \quad (19)$$

795 It is convenient to observed that the $\text{tr}(Q^T \hat{Y}^T Y)$ and $\text{tr}(\hat{X}^T X Q)$ are equivalent with each other in
 796 this case. Then assuming the SVD of $\hat{Y}^T Y$ or $\hat{X}^T X$ are $U^T \Sigma V$ and $V^T \Sigma U$, respectively, then we
 797 have Equation 20.

$$\begin{aligned} \text{tr}(Q^T \hat{Y}^T Y) &= \text{tr}(Q^T U^T \Sigma V) = \text{tr}(Q^T U^T V \Sigma) \\ &= \text{tr}(Z \Sigma) = \sum_{i=1}^p z_{ii} \sigma_i \leq \sum_{i=1}^p \sigma_i \end{aligned} \quad (20)$$

802 With the same reason, we obtain the Equation 21.

$$\begin{aligned} \text{tr}(\hat{X}^T X Q) &= \text{tr}(V^T \Sigma U Q) = \text{tr}(Q^T U^T V \Sigma) \\ &= \text{tr}(Z \Sigma) = \sum_{i=1}^p z_{ii} \sigma_i \leq \sum_{i=1}^p \sigma_i \end{aligned} \quad (21)$$

808 In both equations, Z is an orthogonal matrix defined by $V^T Q^T U$. When Z is an identity matrix, the
 809 upper bound is attained, and it is concluded that when $Q = UV^T$, the optimization problem has been
 solved (Schönemann, 1966).

810 C ADVERSARIAL ATTACK ALGORITHMS
811

812 To evaluate the robustness of BAM trained with different strategy, several widely used adversarial
813 attack algorithms, including FGSM, FFGSM, BIM, and PGD, are used. We will briefly discuss each
814 algorithm in this section.

815 **Fast Gradient Sign Method (FGSM)** (Goodfellow et al., 2014): FGSM is a one-step gradient-based
816 attack that perturbs the input \mathbf{x} in the direction of the gradient of the loss function with respect to the
817 input. The adversarial example is generated as:

$$819 \quad \mathbf{x}^{\text{adv}} = \mathbf{x} + \epsilon \cdot \text{sign}(\nabla_{\mathbf{x}} \mathcal{L}(\theta, \mathbf{x}, y))$$

820 where ϵ controls the perturbation magnitude, and \mathcal{L} is the loss function.

821 **Fast FGSM (FFGSM)** (Wong et al., 2020): FFGSM is a variant of FGSM that adds random
822 initialization before applying the gradient step to increase attack diversity. It introduces a random
823 perturbation $\delta \sim \text{Uniform}(-\alpha, \alpha)$ to the input before computing the FGSM update.

824 **Basic Iterative Method (BIM)** (Kurakin et al., 2018): BIM extends FGSM by applying it iteratively
825 with smaller steps. After each step, the perturbation is clipped to ensure it remains within the ϵ -ball
826 around the original input:

$$827 \quad \mathbf{x}_{t+1}^{\text{adv}} = \text{Clip}_{\mathbf{x}, \epsilon} \{ \mathbf{x}_t^{\text{adv}} + \alpha \cdot \text{sign}(\nabla_{\mathbf{x}} \mathcal{L}(\theta, \mathbf{x}_t^{\text{adv}}, y)) \}$$

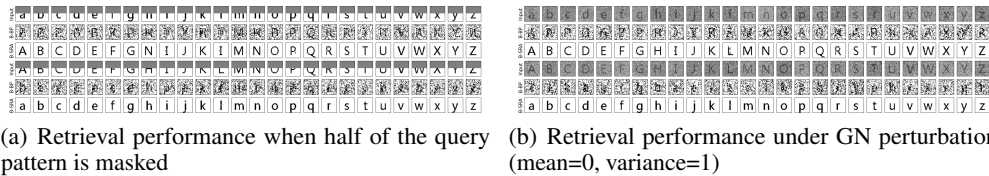
828 **Projected Gradient Descent (PGD)** (Madry et al., 2017): PGD is a stronger version of BIM with
829 random initialization. It applies iterative updates similar to BIM and projects the adversarial example
830 back onto the allowed ℓ_{∞} -ball centered at the clean input:

$$831 \quad \mathbf{x}_0^{\text{adv}} = \mathbf{x} + \delta, \quad \delta \sim \text{Uniform}(-\epsilon, \epsilon)$$

$$832 \quad \mathbf{x}_{t+1}^{\text{adv}} = \Pi_{\mathcal{B}_{\epsilon}(\mathbf{x})} (\mathbf{x}_t^{\text{adv}} + \alpha \cdot \text{sign}(\nabla_{\mathbf{x}} \mathcal{L}(\theta, \mathbf{x}_t^{\text{adv}}, y)))$$

833 D EXTENDED EXPERIMENTAL RESULTS ON BAM ROBUSTNESS
834

835 To further support the findings presented in the main text, this appendix provides additional ex-
836 perimental results that examine the robustness and performance of BAM under a broader range of
837 scenarios. These include extended evaluations across multiple datasets, varying memory capacities,
838 and different adversarial conditions. The goal is to reinforce the key observations regarding the
839 effectiveness of the B-SRA algorithm and the proposed regularization strategies when compared to
840 standard B-BP training.

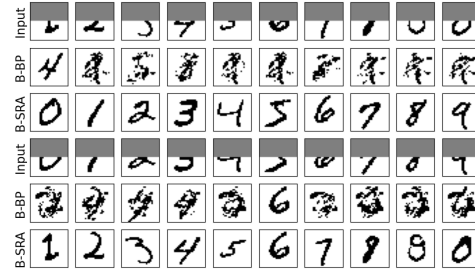
841 D.1 INITIAL EXPERIMENT ON B-SRA AND B-BP
842

843 Figure 5: Association of uppercase and lowercase letters using BAM trained with B-BP and B-SRA

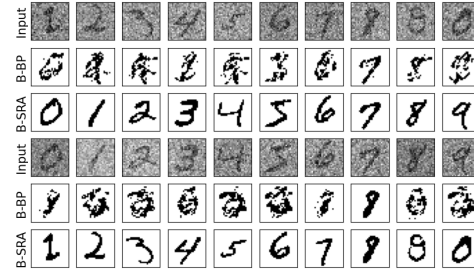
844 To assess the fundamental differences in robustness between B-BP and B-SRA, we conducted a
845 series of initial experiments using three distinct datasets: alphabet letters, MNIST digits, and Chinese
846 script patterns. For each dataset, BAM models were trained using both B-BP and B-SRA, and then
847 evaluated under two adversarial conditions: (i) partially covered patterns (half of the pattern masked),
848 and (ii) Gaussian noise perturbation (mean = 0, variance = 1).

849 As shown in Figures 5, 6, and 7, the BAM models trained using B-BP consistently failed to recover
850 the correct outputs under both covered and noisy conditions, often not retrieving any effective and

864
865
866
867
868
869
870
871
872
873
874
875
876
877
878
879



(a) Retrieval performance when half of the query pattern is masked

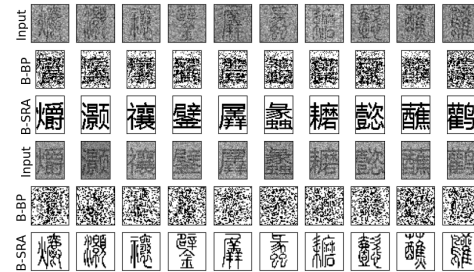


(b) Retrieval performance under GN perturbation (mean=0, variance=1)

880
881
882
883 Figure 6: Association of 20 digital number with another 20 digital number in MNIST dataset using
884 BAM trained with B-BP and B-SRA



(a) Retrieval performance when half of the query pattern is masked



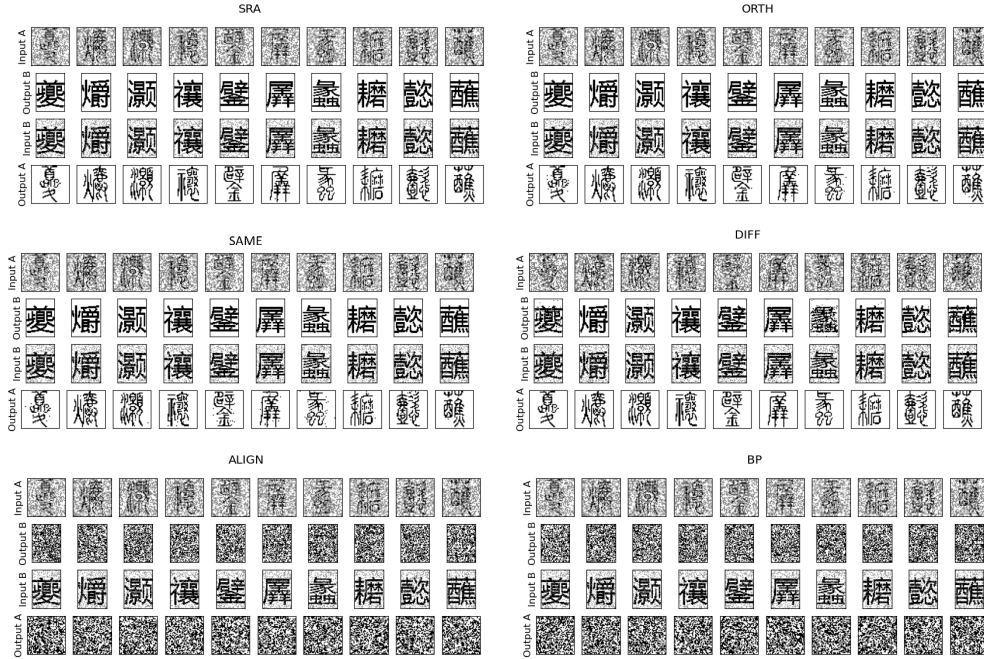
(b) Retrieval performance under GN perturbation (mean=0, variance=1)

910
911 Figure 7: Association of 50 regular scripts with 50 seal scripts using BAM trained with B-BP and
912 B-SRA

913
914
915
916
917

918 clean associated patterns. In contrast, the BAM models trained with B-SRA demonstrated strong
 919 resilience, successfully retrieving the clean and clear associated patterns even when the inputs were
 920 heavily adversarially perturbed. These results highlight the inherent robustness advantage of B-SRA
 921 over B-BP in associative memory tasks.

923 D.2 ABLATION STUDY FOR INDIVIDUAL REGULARIZATION



947 Figure 8: Retrieval performance of BAM trained with different strategies under FGSM attack
 948 ($\epsilon = 0.9$)

951 In this section, we present a comprehensive ablation study using six training strategies—B-BP,
 952 ALIGN, SAME, DIFF, ORTH, and SRA—to evaluate the individual contributions of orthogonal
 953 weight matrix regularization and gradient-pattern alignment to model robustness. These models are
 954 tested under three adversarial attack scenarios: FGSM, FFGSM, and PGD. The corresponding results
 955 are visualized in Figures 8, 9, and 10.

956 It is observed that the models trained with SRA, ORTH, SAME, and DIFF can resist strong FGSM
 957 attacks (Figure 8). Under the more aggressive FFGSM and PGD attacks, only SRA, ORTH, and
 958 SAME maintain robustness (Figures 9 and 10). Among all configurations, the SAME strategy
 959 demonstrates the best overall performance across all attack types.

960 Notably, for these robust training strategies, the adversarial attacks are unable to generate imperceptible
 961 perturbations that deceive the BAM models. To ensure the attack is intensive, we set the attack
 962 parameters (e.g., α , ϵ) to values significantly larger than those typically used against conventional
 963 deep learning models. These findings highlight the inherent robustness of BAM under the SRA,
 964 ORTH, and SAME training strategies and suggest the feasibility of embedding BAM modules into
 965 broader deep learning frameworks to improve their adversarial resilience.

967 D.3 CASE STUDY: ASSOCIATION OF 100 PAIRS OF SCRIPT PATTERNS

969 To further evaluate the robustness of BAM trained with the SRA, ORTH, SAME, and DIFF strategies,
 970 we conducted an additional experiment involving the association of 100 pairs of regular and seal script
 971 patterns. The retrieval performance under two adversarial conditions—partially covered patterns and
 Gaussian noise perturbation—is illustrated in Figures 11 and 12.

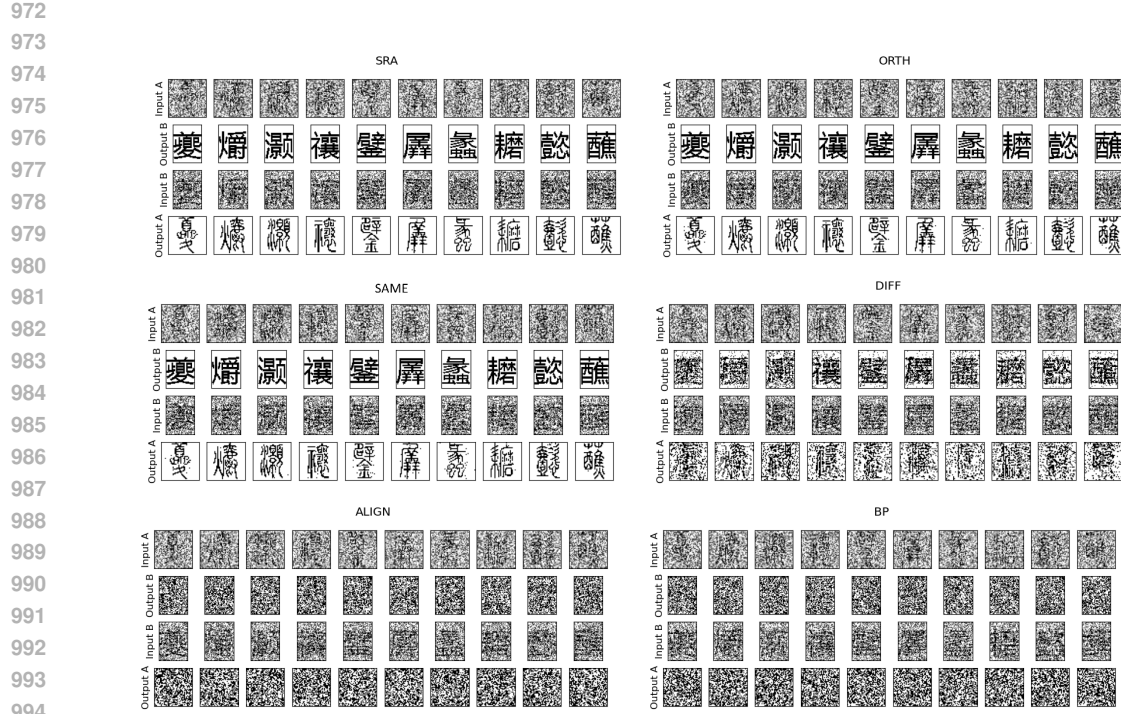


Figure 9: Retrieval performance of BAM trained with different strategies under FFGSM attack ($\alpha = 2, \epsilon = 1$)

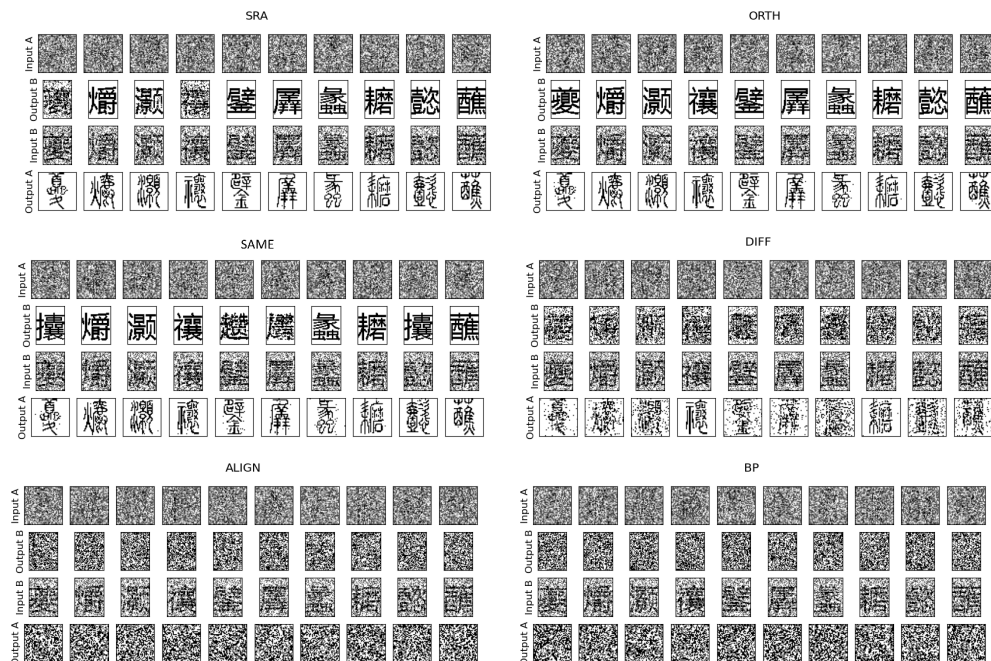
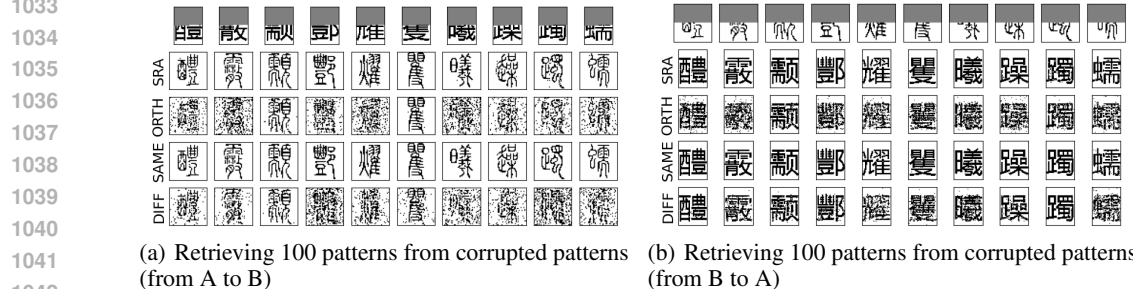
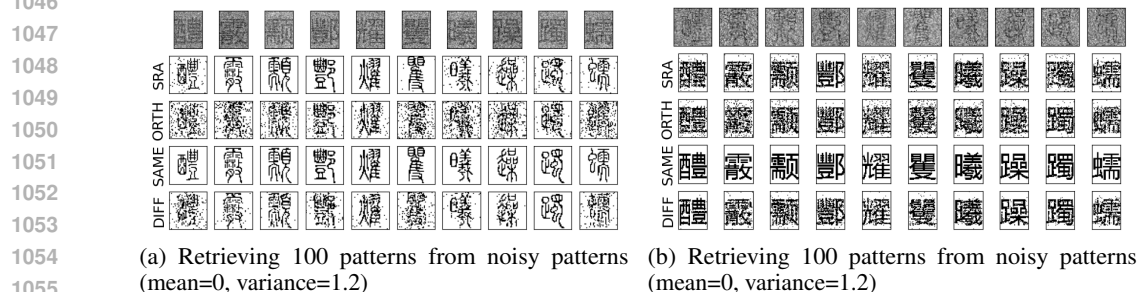


Figure 10: Retrieval performance of BAM trained with different strategies under PGD attack ($\alpha = 2, \epsilon = 0.8, \text{iteration} = 20$)

1026
 1027 It is observed that partially covered patterns remain a relatively weak form of attack for all four
 1028 strategies, with BAM still able to retrieve the associated patterns reliably, as shown in Figure 11.
 1029 However, when Gaussian noise (mean = 0, variance = 1.2) is added to the inputs, performance
 1030 differences become more pronounced. In this case, the SAME strategy clearly outperforms both SRA
 1031 and ORTH, which themselves perform better than DIFF, as shown in Figure 12. These results reaffirm
 1032 the robustness advantage of SAME, especially under more challenging perturbation scenarios.
 1033
 1034

1043
 1044 Figure 11: Retrieving 100 associated patterns from corrupted patterns
 1045
 10461054
 1055 Figure 12: Retrieving 100 patterns from noisy patterns
 1056
 1057

1058 Further experiments will be required to comprehensively evaluate the consistency and limitations of
 1059 these training strategies across more complex datasets and adversarial conditions.
 1060
 1061
 1062
 1063
 1064
 1065
 1066
 1067
 1068
 1069
 1070
 1071
 1072
 1073
 1074
 1075
 1076
 1077
 1078
 1079